1 Hybridized Orbital Ordering Project – Orbital hybridization ordering study in strongly correlated electron systems and the external field effect –

Project Leader: Hironori Nakao

1-1 Introduction

Various intriguing physical properties have been discovered in strongly correlated electron systems (SCES). In such systems, the strong correlation among charge, spin, and orbital of the *3d* electrons and lattice degrees of freedom play important roles. Hence, it is important to study these electronic states in order to understand the phenomena microscopically. Moreover, marked physical properties, such as high T_C superconductivity and colossal magnetoresistance effects, have been often reported near the metal-insulator (MI) transition, where the localized electrons, *d*-electrons in transition metals and *f*-electrons in rare-earth metals, and the itinerant electrons, O*2p*, S*3p*, and so on, compete with each other. For example, superconductors generally exist in the vicinity of a quantum critical point. Hence, it is important to study the orbital hybridized states where itinerancy and localization of electrons compete in order to elucidate the origin of these physical properties. In this project, the hybridized orbital states near the MI transition and in FE compounds were investigated by the complementary use of hard and soft X-rays. The external field (temperature, pressure, magnetic and electric field, and light) effects are an important issue in SCES.

Our research encompasses various subjects such as transition metal oxides, rare-earth metal compounds, and organic conductors, which are typical systems in SCES, and is being performed in collaboration with many external researchers. Here, we report recent studies of photoinduced phase transition in layered manganite [1], new spin-orbital ordering in strained thin film of $LaCoO_3$ [2], and orbital states of V trimers in $BaV_{10}O_{15}$ [3].

1-2 X-ray photoinduced persistent and bidirectional phase transition enabled by impurity doping in layered manganite [1]

Phase transition triggered by light irradiation, or so-called photoinduced phase transition (PIPT), has attracted much interest in the field of photonic and materials science. Many PIPT materials have been found to exhibit novel transient phases not observed in thermal equilibrium. In general, the photoinduced phases are rather unstable and their lifetimes are very short, typically in the order of picoseconds to microseconds. To achieve a persistent photoinduced phase conversion, the initial and final states should be separated by a high potential barrier. If the free energy allows bistability between the initial and final phases, photoexcitation may induce phase conversion beyond the potential barrier between the two phases by the assistance of cooperative interactions in photoexcited states.

Impurity undoped $La_{0.5}Sr_{1.5}MnO_4$ is a typical crystal showing the charge-orbital order (COO) and CE-type antiferromagnetic (AFM) phase with inherent phase competition with the ferromagnetic (FM) metallic phase. In the AFM/COO phase, photo-conversion phenomena have been observed, such as a partial melting of the COO phase by X-ray irradiation, which corresponds to the transition from the COO phase to a charge-orbital disordered (DO) phase. In this study, we investigated X-ray PIPT phenomena in Fe-doped layered perovskite manganite $La_{0.5}Sr_{1.5}Mn_{0.97}Fe_{0.03}O_4$ [Fig. 1]. The substitution of Mn ions with Fe ions would destroy the CE-type AFM order locally and form a small FM cluster, and finally the phase-separated state between the AFM/COO and FM/DO phases would be realized. The doping impurity, as a quenched disorder, may have the effect of enhancing the photo-conversion effect and lowering the threshold for the emergence of PIPT.

It was revealed that 3% doping of Fe for Mn reduces the orbital order (OO) intensity by ~1/30, indicating that only a few percent of the Fe ions, functioning as a quenched disorder, effectively suppress the long-range OO phase. Accordingly, this doping induces a weak ferromagnetism (FM) below 40 K. The produced ferromagnetism is subject to the magnetic field annealing effect, where the value of the saturation moment smoothly increases with an increase in the annealing magnetic field, which is generic of phase-separated states.

We found that impurity doping leads to dramatic enhancement of the X-ray induced effect. As shown in Fig. 2, the OO intensity for (1/4 7/4 0) reflection decreases during X-ray exposure with negligible incubation time and remains constant while X-ray irradiation is off at 10 K. The ac susceptibility is enhanced during X-ray exposure at 10 K, indicating that X-ray PIPT corresponds to phase conversion from the OO phase to the FM phase. In contrast, a reverse phase conversion from the FM phase to the OO phase was observed at 70 K [Fig. 2]. As a consequence, this material exhibits persistent and bidirectional X-ray

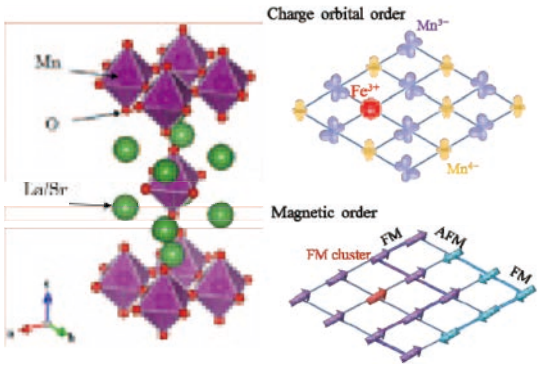

Fig. 1: Schematic of crystal structure of layered perovskite manganite $La_{0.5}Sr_{1.5}MnO_4$, and charge-orbital and CE-type antiferromagnetic order in $La_{0.5}Sr_{1.5}Mn_{0.97}Fe_{0.03}O_4$.

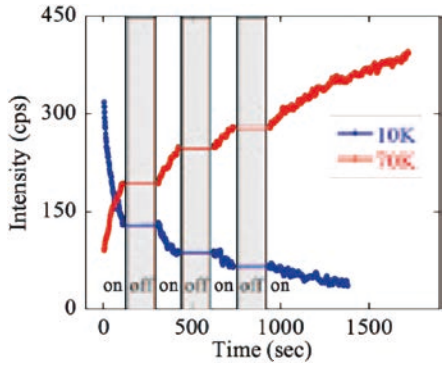

Fig. 2: The X-ray exposure time dependence of the intensities for (1/4 7/4 0) reflections measured at 10 K and 70 K.

induced phase transition, whose direction switches with varying temperature.

The initial state can be considered to be a metastable state protected by a potential barrier from which the incident X-ray can induce transition to the thermodynamically stable state. Switching of the direction of X-ray PIPT can be elucidated by postulating an alteration of the most stable state with varying temperature. In the present case, impurity doping plays a crucial role in forming the phase separated state and also in determining the rate of X-ray PIPT. Tuning of the impurity concentration and selection of the dopant element may provide fertile ground for X-ray PIPT phenomena and for the discovery of new PIPT materials.

1-3 Spin-orbital ordering in strained thin film of $LaCoO_3$ [2]

The interplay among charge, spin and orbital degrees of freedom in strongly correlated electron systems provides a unique arena in which to produce emergent quantum states such as multiferroelectricity and unconventional superconductivity. The perovskite $LaCoO_3$ is known as a prototype of the spin-state crossover material and has attracted much attention in recent decades [4,5]. In this system, the nominally trivalent Co-ion (Co^{3+}) may take three different spin states as shown in Fig. 3(a): the low-spin (LS) state with filled *3d* t_{2g} manifold (S = 0), intermediate-spin (IS) state with active e_g and t_{2g} orbital degrees of freedom (S = 1), and high-spin (HS) state with active t_{2g} orbital degree of freedom (S = 2). Although the ground state is a nonmagnetic phase with LS-state in the bulk form as shown in Fig. 3(b), it has been reported that spontaneous magnetization is observed in the epitaxial thin film of $LaCoO_3$ while keeping its insulating nature [6,7]. Several models have been proposed to explain the strain induced magnetization: the chemically inhomogeneous state including ferromagnetic metallic patches originating from unintentionally doped carriers or the ferromagnetism mediated by the orbital ordering. However, to the best of our knowledge, there is no experimental report exploring the microscopic spin-orbital structure for this enigmatic magnetic phase. Here, we investigated the spin-orbital state for the epitaxial thin film of $LaCoO_3$ by magnetization measurements and resonant X-ray diffraction.

A single crystalline film (60 nm thick) of $LaCoO_3$ was fabricated on the $(LaAlO_3)_{0.3}(SrAl_{0.5}Ta_{0.5}O_3)_{0.7}$ (LSAT) substrate with (110) orientation by pulsed laser deposition. Synchrotron-radiation X-ray diffraction was performed to detect the fundamental and superlattice reflection at BL-3A and BL-4C, Photon Factory of KEK, Japan.

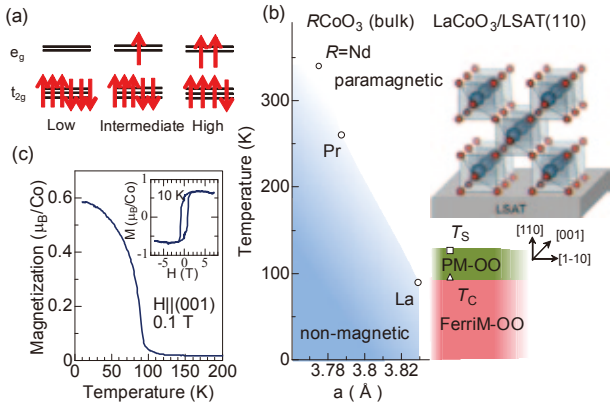

Fig. 3: (a) Schematic view of the spin states of Co^{3+}. (b) Electronic phase diagrams of the tensile strained $LaCoO_3$ and the bulk $RCoO_3$ (*R* is rare-earth element). The circles indicate the typical spin-state crossover temperature from nonmagnetic to paramagnetic state. The square and triangle denote the transition temperature of orbital ordering (OO) and that of ferrimagnetic (FerriM) ordering, respectively. (c) Temperature dependence of in-plane magnetization. Inset shows the in-plane magnetization (M) curve at 10 K.

Figure 3(c) shows the temperature dependence of magnetization. Magnetization increases at T_C = 94 K and the spontaneous magnetization is about 0.7μ_B/Co at 10 K. Figure 4(a) shows the temperature dependence of the out-of-plane lattice constant (d_{110}). As the temperature is lowered, d_{110} steeply decreases down to 126 K and shows minimal temperature dependence below 126 K. Moreover, we have identified a superlattice reflection characterized by the propagation vector q = (1/4, -1/4, 1/4) below 126 K. Figure 4(c) exemplifies the profile of superlattice reflection at (5/4, 3/4, 1/4). The intensity gradually increases below 126 K and nearly saturates below T_C [Fig. 4(b)].

These results point to the existence of the structural phase transition at 126 K (T_S), which quadruples the unit cell of pseudo-cubic setting along the [100], [010] and [001] axes. On the basis of the resonant X-ray scattering at the Co *K*-edge, we attributed this structural phase transition to the ordering of Co-*3d* orbital with IS- or HS-state.

Figure 4(d) shows one plausible model of spin-orbital ordering; the spin and orbital alignment is viewed as the stacking of two-dimensional sheets of IS- and HS-state sites in the order of IS ↑ -IS ↑ -HS ↓ -IS ↑ … spin configuration with $d_{z2\text{-}x2}$-$d_{x2\text{-}y2}$-d_{yz}-$d_{x2\text{-}y2}$ … orbital configuration along the [1 -1 1] direction. This model is also consistent with the observed net magnetization and result of resonant soft X-ray diffraction [8].

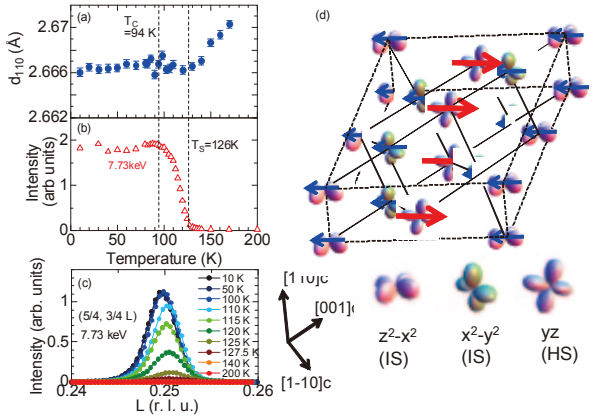

Fig. 4: Temperature dependence of (a) d_{110} and (b) scattering intensity of (5/4, 3/4, 1/4) reflection. (c) Profile of (5/4, 3/4, 1/4) reflection. (d) A plausible model of spin-orbital ordering.

1-4 Orbital states of V trimers in $BaV_{10}O_{15}$ detected by resonant X-ray scattering [3]

The cluster formation of transition metals as a phase transition has been investigated extensively in various transition-metal compounds. The peculiar cluster formation of three V^{3+} ($3d^2$) ions, i.e., V trimerization, is observed in various vanadates in which V ions form triangle-based lattices, such as $LiVO_2$, $LiVS_2$, NaV_6O_{11}, $BaV_{10}O_{15}$, and $A_2V_{13}O_{22}$ (A = Ba, Sr). Theoretically, Pen et al. proposed a model of t_{2g} orbital ordering of the 3*d* electrons for the V trimerization in $LiVO_2$ [9]. In their model, a bonding state of the t_{2g} orbitals is formed at each side of the V^{3+} triangle, as shown in Fig. 5(a). Experimentally, however, such orbital ordering in the V trimer has not been confirmed yet, even in $LiVO_2$.

$BaV_{10}O_{15}$ shows a structural phase transition associated with the trimerization of V ions at *T*s = 123 K [10]. We investigated the orbital states of V trimers in $BaV_{10}O_{15}$ using the technique of resonant X-ray scattering (RXS) near the V *K*-edge absorption energy. RXS is an excellent probe to investigate the orbital states in transition-metal oxides, since it can detect both the local site symmetry and modulation of the electronic states in transition metals by quantitative analysis of the reciprocal *Q* position dependence in the RXS signal [11].

X-ray scattering measurements were performed at BL-4C at the Photon Factory. The energy resolution was ~3 eV. The incident X-ray beam had σ polarization in the present experimental configuration, as illustrated in Fig. 5(b). As a result, we detected the resonant signals of the scattering only below *T*c, corresponding to the trimer formation of the structure in the low-temperature phase [Fig. 5(c)].

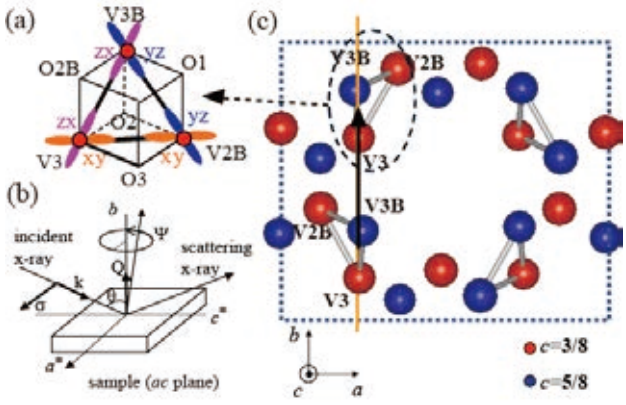

Fig. 5: (a) Model of the orbital order in V trimer. (b) Schematic layout for RXS. (c) Arrangements of the V ions for $BaV_{10}O_{15}$. The bars connecting the circles represent the V-V bonds in trimers. The *b* glide on the *bc* plane is indicated by the solid line.

Figure 6(a) shows the photon-energy dependence of the RXS signal. Three distinct peak structures (labeled A, B, and C) are observed on the photon-energy dependence at the (010), (030), and (050) reflections. The structure A is the pre-edge structure corresponding to the threshold of the 1*s* to 3*d*

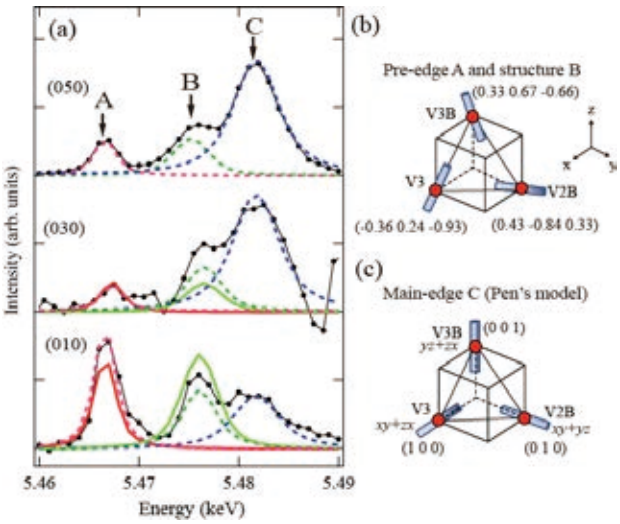

Fig. 6: (a) Photon energy dependence of RXS at Q = (010), (030) and (050). The fitting results for the structures A, B and C are indicated by the dashed lines. The intensities calculated from the model analysis are also plotted (solid lines). (b) Principal axes of the ASF tensors for the 1*s* to 3*d* and to 4*s* transitions. (c) Principal axes for the 1*s* to 4*p*.

transition of the V sites, while the structure C is the main-edge structure corresponding to the threshold of the 1*s* to 4*p* transition. The energy of the structure B can be ascribed to the 1*s* to 4*s* transition. As seen in Fig. 6(a), the intensity ratios of I_A/I_C (and I_B/I_C) at (010) are larger than those at (030) and (050), indicating that the pre-edge signal is enhanced at (010).

The RXS intensity is dominated by the atomic scattering factor (ASF) tensors. The present experiment result indicates that the ASF tensor is different in the pre-edge A (or structure B) region and the main-edge C region. Such a difference arises from the different origins of the ASF tensors in the V ion for the pre-edge A (and structure B) and main-edge C.

As to the pre-edge A and structure B, the anomalous scattering mainly comes from the local centro-symmetry breaking of the V ions in a VO_6 octahedron. In this situation, the anisotropic part of ASF is proportional to the projections of this dipole onto the *a* and *b* axes. This is equivalent to saying that the principal axis of the ASF tensor for the pre-edge A and structure B is along the electric dipole direction. The dipole direction for the V3B, V3, and V2B sites corresponds to the shift of the V atoms from the center of the octahedron and can be estimated to Fig. 6(b).

On the other hand, the ASF tensor for the main-edge peak C is dominated by the energy splitting of the 4*p* states [4]. When the *yz* and *zx* states of V 3*d* orbitals are occupied, the p_z state of V 4*p* orbitals is split from the p_x and p_y state. In this case, the principal axis of the ASF tensor is along the local *z* direction. In the model of the orbital ordering by Pen et al., d_{zx}, d_{yz} are occupied in V3B, d_{zx}, d_{xy} are occupied in V3, and d_{yz}, d_{xy} are occupied in V2B. Therefore, the directions of the principal axes for the ASF tensors of V3B, V3 and V2B are (0,0,1), (1,0,0), and (0,1,0), respectively [Fig. 6(c)].

From these directions of the ASF tensors, the Q dependence of RXS intensity was calculated. The calculated relative intensities I_A/I_C and I_B/I_C for (010) and (030) are plotted by solid lines in Fig. 6(a). The relative intensities I_A/I_C and I_B/I_C for (010) and (030) are well reproduced by the present model. The results of the model analysis of the Q dependence are consistent with the orbital order proposed by Pen et al. and also the results of LDA band calculations.

References

[1] Y. Yamaki et al., Phys. Rev. B **87**, 081107(R) (2013).
[2] J. Fujioka et al., Phys. Rev. Lett. **111** (2013) 027206.
[3] K. Takubo et al., Phys. Rev. B **86** (2012) 085141.
[4] P. M. Raccah and J. B. Goodenough, Phys. Rev. **155**, 932 (1967).
[5] M. A. Korotin et al., Phys. Rev. B **54**, 5309 (1996).
[6] D. Fuchs et al., Phys. Rev. B **75**, 144402 (2007).
[7] J. W. Freeland, J. X. Ma, and J. Shi, Appl. Phys. Lett. **93**, 212501 (2008).
[8]Y. Yamasaki et al., unpublished.
[9] H. F. Pen et al., Phys. Rev. Lett. **78** (1997) 1323.
[10] T. Kajita et al., Phys. Rev. B **81** (2010) 060405(R).
[11] H. Nakao et al., Phys. Rev. B **66** (2002) 184419.